Mechanisms of *Igf2* inhibition in thymic epithelial cells infected by coxsackievirus CV-B4

Hélène Michaux[a#], Aymen Halouani[b], Charlotte Trussart[a], Chantal Renard[a], Hela Jaïdane[b], Henri Martens[a], Didier Hober[c], Vincent Geenen[a]

[a]Neuroimmunoendocrinology, Université de Liège GIGA Institute, Liège-Sart Tilman, Belgium

[b]Laboratoire des Maladies Transmissibles et Substances Biologiquement actives LR99ES27, Université El Manar (Tunis) and Université de Monastir, Monastir, Tunisia

[c]Laboratoire de Virologie EA3610, Université de Lille, Lille, France

Runing title

Transcriptional decrease of *Igf2* in CVB4 infected TECs

#Corresponding author:

Hélène Michaux, PhD

hmichaux88@gmail.com

Keywords: Thymus – Thymic epithelial cell (TEC) – Type 1 diabetes (T1D) – Coxsackievirus B4 (CV-B4) – Insulin-like growth factor 2 (IGF2/*Igf2*) – Transcription

Word count: Abstract 182. Importance 149. Text 5519. References 60. Figures 6

ABSTRACT

Epidemiological studies have evidenced a link between type 1 diabetes (T1D) and infections by enteroviruses, especially with coxsackievirus B4 (CV-B4). CV-B4 is able to infect human and murine thymic epithelial cells (TECs) and, in a murine TEC line, we have shown that the diabetogenic strain CV-B4 E2 decreases transcription of insulin-like growth factor 2 gene (*Igf2*), coding for the self-peptide of the insulin family. Here we show that in CV-B4 infection of mice alters *Igf2* transcripts isoforms in TECs, followed by a decrease of pro-IGF2 precursor in the thymus. CV-B4 infection of a murine TEC line decreases *Igf2* P3 promoter activity by targeting the region -68 to -22 upstream of the transcription start site (TSS) whereas *Igf2* transcripts stability is not affected, pointing towards a regulation of *Igf2* transcription. Our data also show that CV-B4 decreases IL-6/STAT3 signaling *in vitro*. This study provides new knowledge about the regulation of intrathymic *Igf2* transcription by CV-B4 and reinforces the hypothesis that CV-B4 infection of the thymus could break central self-tolerance of the insulin family by decreasing *Igf2* transcription and IGF2 presentation in thymus epithelium.

IMPORTANCE

Coxsackievirus B4 represents one of the most important environmental factors associated to type 1 diabetes, autoimmune disease for which no curative treatment exist. The diabetogenic strain Coxsackievirus B4 E2 was previously shown to decrease *Igf2* expression, important player for central tolerance towards insulin, in a thymic epithelial cell line. The understanding of *Igf2* regulation mechanisms during coxsackievirus B4 infection represents an interest for the understanding of central tolerance development but also for *Igf2* transcriptional regulation itself, still poorly understood.

Here we demonstrate that, some transcripts isoforms of *Igf2* are also decreased in thymic epithelial cells *in vivo*. Moreover, we show that this decrease is induced by an alteration of specific regions of *Igf2* P3 promoter and may be linked by a decrease of STAT3 signaling. *In fine* we hope that this work could lead to future therapies leading to reprogramming central tolerance towards β cells antigens via *Igf2* expression.

INTRODUCTION

The presentation of neuroendocrine self-peptides by thymic epithelial cells (TECs) plays an essential role in programming immune self-tolerance to neuroendocrine functions and a defect in this process is the earliest event in the pathogenesis of autoimmune diseases such as type 1 diabetes (T1D) (1). Insulin-like growth factor 2 (IGF2) is the self-peptide of the insulin family and *Igf2* transcription is absent in the thymus of an animal model of T1D, the diabetes-prone Bio-Breeding (DP-BB) rat (2). Furthermore, *Igf2* expression is required for the establishment of complete immune self-tolerance of insulin (3).

Enteroviruses and especially coxsackievirus B (CV-B) are among the most important environmental factors that have been linked to T1D (4). *Enterovirus* genus is part of the *Picornaviridae* family. Enteroviruses are non-enveloped small viruses, composed of a single-strand positive RNA in an icosahedric capsid and are transmitted by orofecal route. The so-called diabetogenic strain CV-B4 E2 has been isolated from a child died from ketoacidosis after an acute T1D onset (5). CV-B4, frequently detected in T1D patients, has a tropism for pancreatic insulin-secreting β cells in Langerhans islets and various mechanisms were proposed to explain the induction of autoimmune T1D by enteroviruses (4).

For several years we have been investigating whether CV-B4 could infect the thymus and disturb its crucial function in the programming of central self-tolerance to the insulin family and to islet β cells. Following oral and intra-peritoneal inoculation, CV-B4 also infects the thymus, which leads to abnormal T-cells differentiation (6-9) and this was also observed in murine and human thymic fetal organ cultures (10, 11). Also, CV-B4 is able to induce a persistent infection of primary cultures of human TECs and to modulate their profile of

77 cytokine secretion (12). CV-B4 persistently infects the MTE4-14 cell line, a TEC line
78 derived from neonatal mice (13), and this induces a drastic decrease in *Igf2* transcription
79 and IGF2 production while *Igf1* transcription was much less affected (14).

80 In this study, we investigated the effects of CV-B4 E2 infection on *Igf2* transcription using
81 an enrichment method of TECs (15, 16) from an outbred susceptible mice strain (9). We
82 also explored mechanisms of the regulation of *Igf2* transcription in MTE4-14 cells induced
83 by a short CV-B4 infection.

84

RESULTS

CV-B4 E2 decreases *Igf2* transcripts and pro-IGF2 expression in TECs *in vivo*

Igf2 is mainly found in TECs (CD45-), which encompass only a few percent of the thymic population. We decided to use for each thymus a depletion of thymocytes based on their positive CD45 expression to enrich in $CD45^-$ TECs (**Fig. 1A and 1B**). TECs ($CD45^-EpCAM^+$) were enriched in average 62-fold in $CD45^-$ sorted cells and accordingly, *total Igf2* mRNA relative level was in average 318-fold higher in $CD45^-$ sorted cells (TECs) compared to total thymic cells (**Fig. 1C**).

We investigated *Igf2* expression by RT-qPCR in TECs. It is known that murine *Igf2* gene contains three main promoters (P1, P2, P3) which give rise to three transcript isoforms differing only in their first exon (5'UTR): *Igf2 V3* (*Igf2* P3), *Igf2 V1* (*Igf2* P2), and *Igf2 V2* (*Igf2* P1) (17). *Igf2* Variant 3 *(Igf2 V3)* and *Igf2* Variant 2 mRNA *(Igf2 V2)* isoforms, main and minor *Igf2* transcripts isoforms respectively (**Fig. 1D**), were significantly decreased at 2 days post-infection (P.I.) in infected mice. However, *Igf2* Variant 1 *(Igf2 V1)* was on the opposite upregulated by CV-B4 E2 after 3 days P.I., and *total Igf2* in TECs was not significantly decreased in CV-B4 E2 inoculated mice. At 7 days P.I., relative expression for each isoform returns to comparable level to mock-inoculated mice (**Fig. 1E**).

Next, IGF2 protein level and its precursors were analyzed in total thymic cell population (containing both thymocytes and TECs) by Western Blot. Mainly pro-IGF2 precursor form (18 kDa, dominant isoform) was detected whereas no mature IGF2 was observed. Interestingly, compared to mock-inoculated mice, pro-IGF2 level was significantly decreased during the course of the infection, especially at day 7 P.I (**Fig. 1F**). Collectively, these results suggest that CV-B4 is able to decrease *Igf2* at mRNA and protein level in the

thymus. Of note, despite evident sign of CV-B4 infection detected in all pancreases sampled from CV-B4 inoculated mice, CV-B4 viral RNA was surprisingly not detected within thymic cells (**Fig. 1G**).

CV-B4 E2 decreases *Igf2* transcripts and pro-IGF2 expression in MTE4-14 cell line

Among *Igf2* transcripts, only *Igf2 V1* and *Igf2 V3* mRNA are detected by RT-PCR in MTE4-14 cell line (**Fig. 2A**) with a large dominant expression of *Igf2 V3* (**Fig. 2B**). During the course of CV-B4 $_{MOI = 0.05}$ infection, RT-qPCR results show a significant and gradual decrease of *total Igf2*, starting at day 2 P.I. Moreover, among *Igf2* mRNA transcripts, both *Igf2 V3* and *Igf2 V1* were decreased of 74% at day 3 P.I. in CV-B4 $_{MOI = 0.05}$ infected cells (**Fig. 3A**). Regulator of cell cycle *Tp53,* and apoptosis regulators *Birc5* and *Bax,* previously shown to be modulated during enterovirus or by others single-stranded positive RNA viruses (18-20), were not altered during the time course of infection with CV-B4 $_{MOI = 0.05}$ (**Fig. 3B**).

Protein level of IGF2 and its precursors were investigated by Western Blot as in Fig. 1. As shown above *in vivo*, no mature IGF2 was detectable in mock and in CV-B4 $_{MOI = 0.05}$ infected cells. As in Fig. 1F, we were able to detect mainly pro-IGF2 at a molecular weight comparable as in the thymus *in vivo*. During the time course of infection in MTE4-14, pro-IGF2 decreased gradually, especially at day 3 P.I. where a loss of 51% was measured in CV-B4 $_{MOI = 0.05}$ infected cells (**Fig. 3C**).

Together these results show that CV-B4 is able to decrease both at mRNA and protein level IGF2 in MTE4-14 cell line. Of note as *Igf2* expression decreases, a concomitant increase of CV-B4 replication and production can be observed (**Fig. 3D-F**).

CV-B4 E2 decreases *Igf2* P3 promoter activity

We hypothesized that the decrease of *Igf2 V3* mRNA (dominant *Igf2* transcript isoform in MTE4-14 cell line) in CV-B4 E2 infected cells could have a transcriptional origin. For this, we cloned *Igf2* P3 promoter (-168 to +175 relative to the TSS) upstream of Nanoluciferase coding sequence in a reporter vector (**Fig. 4A**). Whereas *Igf2* P3 promoter activity is unchanged at day 1 P.I., results show a significant decrease of *Igf2* P3 promoter activity at 2 days P.I. of 38% in CV-B4 $_{MOI = 0.05}$ infected cells. Moreover, this effect increases as the CV-B4 multiplicity of infection increases (**Fig. 4B**). To further determine whether the *Igf2* decrease in infected cells has a post-transcriptional origin, we analyzed by RT-qPCR *Igf2 V3* mRNA expression followed by actinomycin D treatment at 2 days P.I. However, this analysis did not reveal a significant difference of *Igf2 V3* mRNA stability between mock and CV-B4 infected cells even after 10 hours of treatment; mRNA half-life was estimated at 8.6 h and 9.5 h respectively in mock and in infected cells (**Fig. 4C**). Together these results exclude the possibility that CV-B4 plays a significant role at the post-transcriptional level on *Igf2* expression and indicate that *Igf2* mRNA decrease is rather associated with a decrease of *Igf2* P3 promoter activity.

Proximal promoter contains multiple binding sites specific for diverse transcription factors. To identify binding sites of *Igf2* P3 (-168 to +175 relative to the TSS) that play a role in the decrease of *Igf2* P3 promoter activity, we created a series of truncation constructs and tested them at day 2 P.I. in a transient luciferase reporter system as above (**Fig. 5A**). In mock and in CV-B4 $_{MOI = 0.05}$ infected cells, the progressive deletion in *Igf2* P3 (-168 to +175) induced a gradual decrease of promoter activity, until the construct P197 (-22 to +175) where no promoter activity was detectable in all conditions (**Fig. 5B**). Similar results

were obtained with constructs containing *Igf2* P3 promoter containing sequence downstream -22 (data not shown), identifying the region -168 to -22 as essential for *Igf2* P3 promoter minimal activity. Promoter activity of the construct P243 (-68 to +175) and P230 (-55 to +175) were significantly decreased in infected cells (**Fig. 5C**), while construct P291 (-116 to +175) did not reveal any significant change in infected cells indicating that the region -68 to -22 is downregulated by CV-B4 $_{MOI = 0.05}$. To explore if the region -168 to -116 plays a role in the decrease of *Igf2* P3 promoter activity, we realized the construction P248* containing the region -168 to -116 but not the region -116 to -22. Although this region represents less than 10% of *Igf2 P3* promoter activity, we were able to detect a significant decrease of *Igf2* P3 promoter activity with the construct P248* in infected cells revealing that the region -168 to -116 is also downregulated by CV-B4 $_{MOI = 0.05}$. We noticed that in the presence of the construct P307 (which do not contain the region -151 to -116) promoter activity in mock cells was significantly higher (p = 0.0242) than with the full *Igf2* P3 promoter (-168 to -116) revealing presence of potential negative regulator element in the region -151 to -116. However, results show that this element in this region does not play a role in infected cells compared to the full promoter (**Fig. 5C**).

We used then bioinformatics prediction software (21) to search for corresponding transcription factor which could bind to the region -68 to -22, representing the main region affected by CV-B4. Several putative binding sites for transcription factors were identified in this region (**Table 1**), as one binding site for the transcription factor Specificity Protein (SP) family, one for Krüppel-Like Factors family (KLFs), and one binding site for Zinc Finger Protein 263 (ZFP263). Binding sites for ZFP263, SP family were also identified in the region -168 to -116 (**Table 1**).

177 **CV-B4 E2 alters IL-6/STAT3 signaling and decreases STAT3 phosphorylation**

178 Given that Signal transducer and activator of transcription 3 (STAT3) acts as positive
179 regulators of *Igf2* transcripts in human and in mice (22, 23), STAT3 protein expression and
180 phosphorylation (STAT3 ^{pY705}) level were analyzed by Western Blot. Results show that
181 CV-B4 $_{MOI = 0.05}$ decreases gradually STAT3^{pY705} during the course of the infection,
182 whereas STAT3^{total} was not significantly affected. STAT3^{pY705} was decreased of 51% and
183 65% respectively at 2 and 3 days P.I. (**Fig. 6A**). In line with this result, *Bcl2,* a STAT3
184 response gene (24), was similarly decreased during the time course of CV-B4 infection in
185 MTE4-14 (**Fig. 6B**).

186 However, *Il6*, activator of *STAT3* ^{pY705}, was upregulated in infected cells (**Fig. 6C**) which is
187 in discordance with the observed decrease of STAT3^{pY705}. We then investigated
188 expression of the receptor IL6Rα (CD126) by flow cytometry but we were not able to
189 detect a significant difference between mock and infected cells (**Fig. 6D**).

190 Previous reports indicate that suppressor of cytokine signaling 3 (SOCS3), a negative
191 regulator of STAT3 activation, is induced by CV-B3 (25, 26). SOCS3 protein expression
192 was analyzed by Western Blot and was not upregulated during the infection. On the
193 opposite, SOCS3 protein level tends to decrease during the infection (**Fig. 6E**). More
194 recently shown to play a negative role in STAT3^{pY705} activation (27-30), expression of the
195 c-Jun N-terminal Kinase (JNK) and the Extracellular signal-Regulated protein Kinase
196 (ERK) were analyzed in MTE4-14 infected cells. At 2 days P.I., we observed that
197 phosphorylated JNK and phosphorylated ERK were both increased whereas level of
198 JNK^{total} or ERK^{total} remained unchanged (**Fig. 6F-G**).

199

DISCUSSION

In this research, we firstly investigate the effect of CV-B4 E2 on *Igf2* expression in murine TECs *in vivo*. The analysis of *Igf2* transcripts isoforms in mock inoculated mice revealed that *Igf2 V3* and *Igf2 V1* are the isoforms which can be mainly detected in $CD45^-$ enriched TECs. These results corroborate with previous reports on human TECs showing that *IGF2* P3 and *IGF*2 P4, homologous promoter of *Igf2 V1* and *Igf2 V3* respectively are active in these cells (31) and accordingly, much less *Igf2 V2* in $CD45^-$ enriched TECs was detected. In CV-B4 inoculated mice, both *Igf2 V3* and *Igf2 V2* were decreased followed by an upregulation of *Igf2 V1*. These results explained why *total Igf2* (representing quantitatively sum of all *Igf2* isoforms) was not decreased in infected mice and indicate a differential regulation of *Igf2* mRNA transcripts in the thymus by CV-B4 E2. Thus, distinct pathways may regulate *Igf2 V3* and *V1* mRNA isoforms during CV-B4 infection. This temporal decrease of *Igf2 V3* and *Igf2 V2* was nevertheless sufficient to achieve a later significant decrease of Pro-IGF2. Consequently a role of CV-B4 on IGF2 presentation in the thymus cannot be excluded**,** indeed it was shown that CV-B3 is able to alter class I antigen presentation (32). Nevertheless, we were not able to detect any mature IGF2 neither in the thymus nor in the TEC cell line MTE4-14. A differential processing of IGF2 may occur in the thymus. It was reported that in rat, mature forms of IGF2 are also not found in the brain (33). Moreover, sequencing data of TECs indicates low mRNA expression level of protein convertase PC4 (*Pcsk4*), enzyme cleaving pro-IGF2 in mature IGF2. A low thymic expression of *Pcsk4* would affect IGF2 processing and would allow only the detection of IGF2 immature precursors (34, 35). In mice inoculated with CV-B4, we were able to detect CV-B4 RNA in the pancreas. However, CV-B4 RNA was not

223 detected in the thymus which is in discordance with previous reports reporting the
224 presence of CV-B4 RNA in the whole thymus (9, 36). It is likely that the method we
225 employed here for TECs enrichment has interfered negatively with the detection of
226 CV-B4 as it only allows to detect CV-B4 RNA within the cells (**Table 2**). Nonetheless, this
227 result indicates that CV-B4 could not replicate as much as expected within murine thymic
228 cells. Of note, attempts to detect CV-B3 replication within cells of murine thymus have
229 similarly failed (37, 38).

230 Interestingly, several reports show that interferon (IFN)-α or IFN-β are able to decrease
231 *Igf2* expression (39-41) and that inactivated CV-Bs virions, by interacting with
232 extracellular Toll-like receptors (TLRs), can still upregulate these interferon suggesting
233 that no replication within cells is actually required to induce IFN expression (42). Thus,
234 CV-B4 draining not replicative virions, within the thymus could induce via TLRs IFN-α or
235 IFN-β which may then alter *Igf2* transcripts.

236 The second objective of this study was to explore mechanisms of *Igf2* decrease in
237 MTE4-14 cells infected with CV-B4 E2. Similar to the results obtained *in vivo, Igf2 V3* and
238 *Igf2 V1* are both detected in the cell line with a dominance of *Igf2 V3* reflecting a
239 dominant activity of *Igf2 P3* and a lower activity of *Igf2 P2.* Both *Igf2 V3* and *Igf2 V1* were
240 downregulated concomitantly to the increase of CV-B4 replication and production. Given
241 that *Igf2 V1* was on the opposite increased *in vivo* and CV-B4 E2 viral RNA not replicative
242 (or under the limit of detection) within murine thymic cells, a differential regulation
243 scenario of *Igf2 V1* isoforms, possibly related to CV-B4 replication, might takes place in
244 the MTE4-14 cell line, where a higher rate of CV-B4 replication occurred.

245 In this study, we demonstrate that the decrease of *Igf2 V3* major isoforms is due to a

246 decrease of *Igf2 P3* promoter activity (-168 to +175 relative to the TSS) revealing a
247 downregulation of *Igf2 V3* at the transcriptional level. *Igf2 V3* mRNA stability was not
248 affected in infected cells which confirm the regulation of *Igf2 V3* mRNA at the
249 transcriptional level. Previous studies on *total Igf2* mRNA stability indicate that *total Igf2*
250 is a highly stable transcript (43, 44). Our results demonstrate also the promoter region of
251 *Igf2 P3* -68 to -22 (relative to the TSS) and secondary the region *Igf2 P3* -168 to -116
252 (relative to the TSS) as regulated negatively by CV-B4. Nonetheless, as we used only
253 CV-B4 $_{MOI = 0.05}$ for this analysis, we can expect that with higher MOI, others *Igf2 P3*
254 promoter regions might be affected. Predictive analysis of *Igf2 P3* -68 to -22 (relative to
255 the TSS) shows binding sites corresponding to transcription factor from the SP/KLF
256 family. Among them, SP1 was accordingly identified as positive activator of human *Igf2*
257 *P4* (homologous to the murine *Igf2 P3* promoter) (45). Besides this, the SP/KLFs
258 transcription factor families were shown to play essential roles in differentiation,
259 development, proliferation or cell death regulation. Interestingly, KLFs transcription
260 factors play a role for thymocytes development (46-48). Further studies would be
261 required to explore *Igf2* regulation by KLFs during CV-B4 infection which could link the
262 observed alteration of thymocytes differentiation (10, 11) and the decrease of *Igf2 V3.*

263 STAT3, playing a role in *Igf2* expression, has been shown recently to be indispensable
264 for TECs development and survivals (49-51). Here in this study, we identified also that
265 CV-B4 decreases STAT3^{pY705} in a thymic epithelial cell line. Moreover, the analysis of the
266 *Igf2 P3* region -168 to -116 (related to the TSS) revealed an E2F binding site which may
267 be recognized by STAT3 (52). It is then possible that the decrease of *Igf2 P3* promoter
268 activity would be linked, at least, in part to a decrease of STAT3^{pY705}. Additionally, as *Il6*

269 was upregulated in infected cells, this work revealed an inhibition of IL-6/STAT3
270 signaling. This upregulation has been previously reported in TECs and in MTE4-14 as
271 well (12, 14). STAT3^{pY705} inhibition was neither not related to an upregulation of SOCS3,
272 nor by an inhibition of IL-6Rα (CD126). On the contrary, we observed a decrease of
273 SOCS3 which can be attributed to the decrease of STAT3 ^{pY705} signaling itself. Our
274 results indicate an upregulation of JNK and ERK phosphorylation. These kinases,
275 important for enterovirus viral progeny release (53-55) can also indirectly contribute to
276 STAT3^{pY705} downregulation (27-30), which suggest that induction of phosphorylated
277 kinases JNK and ERK could contribute to STAT3^{pY705} decrease and potentially plays also
278 a role in the decrease of *Igf2* in MTE4-14 cells infected with CV-B4.

279 Together, these findings bring new knowledge of *Igf2* regulation by CV-B4 in the context
280 of a thymic infection, and further support the idea that CV-B4 may disturb *Igf2* thymic
281 presentation and decrease central tolerance to insulin.

282

METHODS

Cells and virus

The murine thymic epithelial cell line MTE4-14, of medullar origin, derived from C3H/J (*H-2*^{k}) thymic neonatal lobes (13), was grown in complete high glucose Dulbecco's modified Eagle medium (DMEM; Gibco) supplemented with 10% heat-inactivated fetal calf serum (FCS; Gibco), 2 mM L-glutamine (Gibco), 0.1 µg/mL epidermal growth factor (EGF; Sigma-Aldrich), 100 U/mL penicillin and 100 µg/mL streptomycin (Gibco) (13, 14). VERO cells (kindly provided by the Laboratory of Virology and Immunology, Giga, university of Liège) were grown in DMEM high glucose supplemented with 10% FCS, 100 U/mL penicillin and 100 µg/mL streptomycin. CV-B4 E2, the diabetogenic strain of coxsackievirus B4, (kindly provided by Ji-Won Yoon, Julia McFarlane Diabetes Research Center, Calgary, Alberta, Canada) was propagated in Hela cell line in DMEM high glucose supplemented with 10% FCS. Supernatants were collected 4 days after inoculation, after three freeze/thaw cycles then clarified by centrifugation at 2,500 × g for 10 min, filtered and stored at -80 °C.

Mice inoculation and infection by CV-B4 E2

For *in vivo* experiment, 4–6 weeks old Swiss Albino female mice were used (Janvier Laboratories). Mice were inoculated by intraperitoneal route with either 100 µL of sterile DPBS (DPBS, Dulbecco's Phosphate-Buffered Saline, Thermo Fisher Scientific) for mock-infected mice or with 100 µL of CV-B4 E2 diluted in sterile DPBS at 1.10^{6} $TCID_{50}$/mL. Mice were grouped with a maximum of six per cage, checked and weighted daily. Mice were treated according to general ethic rules with unlimited access to food and water. Six infected and mock-infected animals were sacrificed 2, 3 and 7 days P.I.

306 From each animal, thymus and pancreas were collected. All procedures were approved
307 by the university hospital of Liège ethics committee (Protocol n°13-1611).

308 **TEC isolation, enrichment and immunostaining**

309 Protocol was carried out as previously described (16). Briefly, thymus lobes were cut in
310 small pieces and cleaned for blood and connective tissue in RPMI (Lonza) supplemented
311 with 10% FCS, 2 mM L-glutamine and 100 U/mL penicillin and 100 µg/mL streptomycin
312 (Gibco). Thymic fragments were washed in RPMI 2% FCS and digested 15 min at 37 °C
313 in 500 µg/mL Liberase TL (Sigma-Aldrich) and 111 µg/mL DNase I from bovine pancreas
314 (Sigma-Aldrich). Thymic fragments were mixed in the beginning and in the end of
315 enzymatic digestion. Resulting supernatant was incubated 5 min on ice in DPBS
316 supplemented with 1% FCS and 5 mM EDTA pH7.3. Complete RPMI was added on
317 supernatant and the thymic cell suspension was centrifuged and filtered. Fifty million cells
318 were used for TECs enrichment with mouse CD45 microbeads (Miltenyi Biotec)
319 according to the manufacturer's protocol. For immunostaining, $CD45^-$ enriched cells
320 (TECs) and total thymic suspension was incubated with anti-CD16/CD32 Fc block 1:50
321 (clone 93, eBioscience) during 15 min at 4 °C in MACS buffer followed by incubation with
322 anti-CD45 1:100 (clone 30F-11, BD biosciences), anti-EpCAM 1:100 (clone G8.8,
323 eBioscience) during 30 min. Samples were analyzed on a FACSCanto flow cytometer
324 (BD biosciences) and the raw data analyzed with FlowJo software (Treestar). Purity of
325 CD45 negative sorted cells was in average 80% (data not shown). Aliquots of total thymic
326 cells (digested unsorted cells) were stored for protein and RNA extraction, aliquots of
327 $CD45^-$ isolated cells were stored for RNA extraction.

328

329 **Infection of MTE4-14 by CV-B4 E2**

330 MTE4-14 cells were seeded at 150,000 cells per well on 6-well culture plates in DMEM
331 high glucose supplemented with 10% heat-inactivated FCS, 2 mM L-glutamine, 0.1
332 µg/mL EGF and incubated overnight at 37 °C. The culture medium was then removed
333 and cells were inoculated with 500 µL per well of CV-B4 E2 in DMEM only with a
334 multiplicity of infection (MOI) of 0.05. The MOI is defined by the formula:

335 $$MOI = \frac{Volume\ of\ inoculum\ (mL) * viral\ titer\ \left(\frac{TCID50}{mL}\right) * 0.8}{Number\ of\ cells\ per\ well}$$

336 Alternatively, 2.10^4 MTE4-14 cells were seeded on 96-well culture plates flat bottom and
337 were inoculated with 100 µL per well with various MOI ranging from 0.05 to 5. One well
338 served as control for cell count before infection, allowing similar MOI between
339 experiments. Mock-infected cells served as negative control and were treated under
340 same conditions for all experiments, except inoculation with DMEM alone. After 90 min of
341 incubation cells were washed with DMEM alone, and incubated with complete DMEM
342 without antibiotics for 3 days. At 1 to 3 days P.I., one plate was stopped and processed
343 as follow: culture supernatants were removed and stored at -20 °C for CV-B4 E2 titration,
344 cells were washed, scrapped in PBS then were processed for RNA or protein extraction.

345 **Modified $TCID_{50}$ titration assay**

346 CV-B4 E2 virus titer was determined on VERO cells by a modified Reed and Muench
347 limiting dilution assay as previously described (56, 57). Briefly, after an incubation of 7
348 days with CV-B4 E2 dilutions, cells were incubated during 3 hrs with MTT reagent
349 (Sigma-Aldrich), then formazan was dissolved in DMSO and absorbance was measured
350 at 550 nm. $TCID_{50}$ values (limiting dilution corresponding to 50% of viability) were

obtained by the use of the V_{50} parameter of Boltzmann sigmoid function.

Flow cytometry

For MTE4-14 flow cytometry analysis, cells were harvested with EDTA 5 mM in DPBS during 15 min at 37 °C, washed with 10% FBS before addition of Fc block as described above. MTE4-14 cells were then stained with anti-mouse CD126 APC 1:40 (D7715A7, Biolegend) or with APC rat IgG2b, κ isotype control (Biolegend).

Reverse transcription, end point PCR and real-time quantitative PCR

Total RNA was extracted with Nucleospin RNA kit (Machery Nagel) according to manufacturer's instructions. Alternatively, RNA was extracted with TRIzol Reagent (Ambion) following manufacturer's instructions. If TRIzol was used, contaminating DNA was eliminated with 2 U of DNase Turbo (Ambion) during 30 min at 37 °C, followed by RNA re-extraction with phenol chloroform. RNA concentration was measured on Nanodrop ND-1000 (Thermo Fisher Scientific). $A_{260/280}$ ratio upper than 1.8 were considered as acceptable. Reverse transcription was performed using 200-500 ng of total RNA in the Transcriptor First Strand cDNA synthesis kit (Roche) with 60 µM random hexamer and 6.25 µM oligo$(dT)_{18}$ primer. Reverse transcriptase minus control was used as control for DNA contamination. End Point PCR were realized on an iCycler Thermal Cycler (Bio-Rad) in the presence of GoTaq G2 polymerase (Promega) in 25 µL containing 10-25 ng cDNA, 200 µM dNTPs, 200 nM of each forward and reverse primer, 25 mM $MgCl_2$, 1X Green Buffer and 0.625 U of GoTaq G2 polymerase. The PCR parameters were: one cycle at 95 °C for 2 min; 35 cycles with denaturation at 95 °C for 30 s, annealing at 60 °C for 30 s and elongation at 72 °C for 30 s; one cycle at 72 °C for 5 min. PCR products were visualized on agarose gel. Real time PCR was performed

using Takyon No Rox Sybr 2X masterMix blue dTTp (Eurogentec) with 200 nM of each primer on an iCycler iQ(Bio-Rad). qPCR parameters were: initial denaturation at 95 °C for 10 min; 40 cycles with denaturation at 95 °C for 10 s, annealing at 60 °C for 30 s and amplification at 72 °C for 25 s. Each qPCR reaction was ended by a melting curve with a ramp of 0.5 °C from 55 to 95 °C to control single PCR product amplification. A negative template control for each gene was included in the plate for each mix. Gene expression values were calculated based on the comparative Ct normalized to *Hprt* and displayed as fold change to mock ($2^{-\Delta\Delta Ct}$) or in relative value ($2^{-\Delta Ct}$). Primers (**Table 3-1**) were double checked with PRIMER-BLAST.

One-step CV-B4 E2 RNA detection and two-step CV-B4 E2 RNA detection by PCR

One-step RT-PCR was realized with the SuperScript III One-Step RT-PCR System with Platinum Taq DNA Polymerase (Thermo Fisher Scientific) on an iCycler Thermal Cycler (Bio-Rad). Reactions were performed following manufacturer's instruction containing 500 ng of RNA, 100 nM of 007 and 008 primers. RT-PCR parameters were: one step 50 °C 30 min for cDNA synthesis, followed by one cycle at 94 °C 2 min for initial denaturation; 38 cycles with one cycle 94 °C for 30 s, annealing at 60 °C and extension at 68 °C for 30 s and a final extension at 72 °C for 10 min. PCR products were visualized on agarose gel (1.5%). In case of negative amplification, PCR product was run for a semi-nested PCR for 35 cycles in the presence of Gotaq G2 DNA polymerase as described above. For two-step CV-B4 E2 RNA detection, reverse transcription was performed as described above in 10 µL with 1 µM reverse primer 007 (5′-ATTGTCACCATAAGCAGCCA-3′) for positive strand of CV-B4 E2 or 1 µM forward

primer 008 (5′-GAGTATCAATAAGCTGCTTG-3′) for negative strand detection of CV-B4 E2. PCR amplification was performed then with 100 nM of 007 and 008 primers. PCR parameters were: one cycle at 95 °C for 2 min; 25 cycles with denaturation at 95 °C for 30 s, annealing at 60 °C and extension at 72 °C for 30 s. PCR was ended 5 min at 72 °C. PCR products were analyzed on agarose gel and give a PCR product of 412 bp. Negative PCR was run for semi-nested PCR with internal primer 006 (5′-TCCTCCGGCCCCTGAATGCG-3′) and 007. PCR parameters were: one cycle at 95 °C for 2 min; 35 cycles with denaturation at 95 °C for 30 s, annealing at 60 °C and extension at 72 °C for 30 s. PCR was ended 5 min at 72 °C. Semi-nested PCR product size is 155 bp.

Igf2 P3 Nluc plasmid construction and site-directed mutagenesis

The 342 bp *Igf2* P3 promoter sequence (**Fig. 4A**), containing the proximal promoter of the murine *Igf2* P3 (58, 59) was synthetized by the GeneArt Gene Synthesis service (Thermo Fisher Scientific). TSS sequence was localized with EPD database (60), *Igf2 P3* promoter sequence was then cloned in the Nanoluciferase expressing plasmid pNL1.2 NlucP plasmid (Promega) by the use of restriction site *NheI* (5') and *EcoRV* (3') in *Igf2* P3 promoter by the GeneArt Gene Synthesis service. The resulting plasmid was called *Igf2 P3* Nluc. Site-directed mutagenesis or promoter deletions were performed with the Q5 Site-Directed Mutagenesis Kit (New England Biolabs). PCR reactions were done in 50 µL containing 25 µL of Q5 Hot Start High-Fidelity 2X Master Mix, 500 nM of each forward and reverse primer (**Table 3-2**) and 50 ng of plasmid. The PCR parameters were: one cycle at 98 °C for 30 s; 25 cycles with denaturation step 98 °C for 10 s, annealing (**Table 3-2**) for 30 s and extension step at 72 °C for 150 s and ended at 72 °C for 2 min. Three

annealing temperature were performed in parallel for each primer set. PCR products were loaded on 1% agarose gel with Orange DNA Loading Dye 6X (Thermo Fisher Scientific). SYBR safe (Thermo Fisher Scientific) was added on agarose gel at 1:10,000 for DNA visualization. When single PCR product was detected, KLD mix was added on PCR reaction. Briefly, the KLD reaction contains 2.5 µL 2X KLD buffer, 1 µL of Enzyme Mix, 0.5 µL of PCR product and 0.5 µL of nuclease-free water. Five µL of KLD reaction were mixed with 25 µL of *Escherichia coli* DH5α chemocompetent strain and transformed 45 s at 42 °C. Transformed bacteria were selected on agar plate containing ampicillin at 100 µg/ml. Plasmids were extracted with NucleoSpin Plasmid Transfection-grade (Machery-Nagel) and concentration were measured on Nanodrop ND-1000 (Thermo Fisher Scientific). All plasmids were sequenced by Sanger method (Giga-Genomics).

Transfection and dual luciferase reporter assay on MTE4-14 cell line

Plasmid transfection was performed in 96-well plate. Briefly, each reaction contained 20 µL of 100 ng of pGL3 plasmid (Promega), mixed with 100 ng *Igf2* P3 Nluc (or empty vector or constructs obtained from *Igf2* P3 Nluc), 0.5 µL of Genius DNA transfection Reagent (Westburg) diluted in DMEM. Mix were added directly on 2.10^4 cells/well in a 96-well plate during the seeding. After an overnight incubation at 37 °C, cells were then infected by CV-B4 E2 or DMEM only as described above. Cells were infected during a maximum of two days. Nanoluciferase activity and firefly luciferase activity, were analyzed by the Nano-Glo Dual-Luciferase Reporter Assay System (Promega) following manufacturer's instructions. Bioluminescence was analyzed with a FilterMax F5 (Molecular Devices). Normalized luciferase activity was calculated as the ratio of the Nanoluciferase activity to the firefly luciferase for each sample, then normalized to empty

vector for mock uninfected cells and for CV-B4 E2 infected cells. In each experiment, relative mock value was then set up to 100%.

mRNA stability assay

Actinomycin D (Sigma-Aldrich) was prepared at 1 mg/mL in ethanol and used at 5 µg/mL. mRNA half-life of *Igf2 V3* was estimated by linear regression in each experiment from *Igf2 V3* relative value ($2^{-\Delta Ct}$) (normalized to value of vehicle control for each time point) with the formula $2^{-\Delta Ct(Igf2V3-Hpr\ )} = f(\text{time of actinomycin D treatment})$ for mock or CV-B4 E2 infected cells.

SDS-PAGE and Western Blot

Proteins were extracted in RIPA buffer supplemented with protease and phosphatase inhibitor mini tablets cocktail (Pierce) and stored at -20 °C for further use. Protein extracts were quantified with BCA protein assay kit (Pierce) and denatured at 95 °C during 5 min in Laemmli buffer supplemented with β-mercaptoethanol. Ten µg (or fifty µg for IGF2 detection) of protein lysates were separated on 12% SDS-PAGE gel then transferred to PVDF membrane (Amersham). Transfer was performed at 4 °C during 90 min at 80 V in transfer buffer containing 25 mM Tris, 192 mM glycin and 20% (v/v) methanol. Prior to immunoblotting, membranes were blocked in blocking buffer (5% w/v BSA in TBS-T) during 1 hr at room temperature and primary antibodies **(Table 4**) diluted in blocking buffer were added for overnight at 4 °C. Membranes were then washed three times with TBS-T followed by incubation during 1 hr at room temperature with anti-rabbit or anti-mouse secondary antibody coupled to HRP (all from Cell signaling) diluted at 1:1,000 in blocking buffer. Membranes were then washed three times in TBS-T. Chemiluminescence was visualized with the Pierce ECL Western Blotting Substrate

(Pierce) and acquired on ImageQuant LAS4000 (GE Healthcare). Quantification of band intensity was performed with the ImageJ software. GAPDH or β tubulin was used as loading control and for relative quantification. Positive control for mature IGF2 detection was 500 ng of recombinant mouse IGF2 (R&D Systems).

Statistical analyses

Statistical analyses were performed with GraphPad Prism 8.0. Unpaired *t* test and ratio paired *t* test were used to compare differences between groups, respectively for *in vivo* and *in vitro* experiments. One-way ANOVA was used to compare differences between time points for *in vivo* and *in vitro* experiments. *P* values inferior or equal at 0.05 were considered significant.

CONFLICTS OF INTEREST

The authors declare that they have no conflict of interests.

ACKNOWLEDGEMENTS

This work was supported by doctoral grants obtained from the Fund of Scientific Research (FSR and FRIA of Belgium), by Erasmus+, and by the Fonds Léon Fredericq of Liège University Hospital. The funders had no role in study design, data collection and interpretation, or the decision to submit the work for publication. We thank animal facilities, flow cytometry and also viral vectors platforms from the Institute of Research GIGA at the University of Liège.

488 **REFERENCES**
489

490 1. Geenen V, Trussart C, Michaux H, Halouani A, Jaidane H, Collee C, Renard C,
491 Daukandt M, Ledent P, Martens H. 2019. The presentation of neuroendocrine
492 self-peptides in the thymus: an essential event for individual life and vertebrate
493 survival. Ann N Y Acad Sci doi:10.1111/nyas.14089.

494 2. Kecha-Kamoun O, Achour I, Martens H, Collette J, Lefebvre PJ, Greiner DL, Geenen
495 V. 2001. Thymic expression of insulin-related genes in an animal model of autoimmune
496 type 1 diabetes. Diabetes Metab Res Rev 17:146-52.

497 3. Hansenne I, Renard-Charlet C, Greimers R, Geenen V. 2006. Dendritic cell
498 differentiation and immune tolerance to insulin-related peptides in Igf2-deficient mice. J
499 Immunol 176:4651-7.

500 4. Hober D, Sauter P. 2010. Pathogenesis of type 1 diabetes mellitus: interplay between
501 enterovirus and host. Nat Rev Endocrinol 6:279-89.

502 5. Yoon JW, Austin M, Onodera T, Notkins AL. 1979. Isolation of a virus from the
503 pancreas of a child with diabetic ketoacidosis. N Engl J Med 300:1173-9.

504 6. Bopegamage S, Borsanyiova M, Vargova A, Petrovicova A, Benkovicova M, Gomolcak
505 P. 2003. Coxsackievirus infection of mice. I. Viral kinetics and histopathological
506 changes in mice experimentally infected with coxsackieviruses B3 and B4 by oral
507 route. Acta Virol 47:245-51.

508 7. Bopegamage S, Kovacova J, Vargova A, Motusova J, Petrovicova A, Benkovicova M,
509 Gomolcak P, Bakkers J, van Kuppeveld F, Melchers WJ, Galama JM. 2005. Coxsackie
510 B virus infection of mice: inoculation by the oral route protects the pancreas from
511 damage, but not from infection. J Gen Virol 86:3271-80.

512 8. Chatterjee NK, Hou J, Dockstader P, Charbonneau T. 1992. Coxsackievirus B4
513 infection alters thymic, splenic, and peripheral lymphocyte repertoire preceding onset
514 of hyperglycemia in mice. J Med Virol 38:124-31.

9. Jaidane H, Gharbi J, Lobert PE, Lucas B, Hiar R, M'Hadheb M B, Brilot F, Geenen V, Aouni M, Hober D. 2006. Prolonged viral RNA detection in blood and lymphoid tissues from coxsackievirus B4 E2 orally-inoculated Swiss mice. Microbiol Immunol 50:971-4.

10. Brilot F, Geenen V, Hober D, Stoddart CA. 2004. Coxsackievirus B4 infection of human fetal thymus cells. J Virol 78:9854-61.

11. Brilot F, Jaidane H, Geenen V, Hober D. 2008. Coxsackievirus B4 infection of murine foetal thymus organ cultures. J Med Virol 80:659-66.

12. Brilot F, Chehadeh W, Charlet-Renard C, Martens H, Geenen V, Hober D. 2002. Persistent infection of human thymic epithelial cells by coxsackievirus B4. J Virol 76:5260-5.

13. Lepesant H, Pierres M, Naquet P. 1995. Deficient antigen presentation by thymic epithelial cells reveals differential induction of T cell clone effector functions by CD28-mediated costimulation. Cell Immunol 161:279-87.

14. Jaidane H, Caloone D, Lobert PE, Sane F, Dardenne O, Naquet P, Gharbi J, Aouni M, Geenen V, Hober D. 2012. Persistent infection of thymic epithelial cells with coxsackievirus B4 results in decreased expression of type 2 insulin-like growth factor. J Virol 86:11151-62.

15. Roberts NA, Adams BD, McCarthy NI, Tooze RM, Parnell SM, Anderson G, Kaech SM, Horsley V. 2017. Prdm1 Regulates Thymic Epithelial Function To Prevent Autoimmunity. J Immunol 199:1250-1260.

16. Xing Y, Hogquist KA. 2014. Isolation, identification, and purification of murine thymic epithelial cells. J Vis Exp doi:10.3791/51780:e51780.

17. Bergman D, Halje M, Nordin M, Engstrom W. 2013. Insulin-like growth factor 2 in development and disease: a mini-review. Gerontology 59:240-9.

18. Bok K, Prikhodko VG, Green KY, Sosnovtsev SV. 2009. Apoptosis in murine norovirus-infected RAW264.7 cells is associated with downregulation of survivin. J

Virol 83:3647-56.

19. Chau DH, Yuan J, Zhang H, Cheung P, Lim T, Liu Z, Sall A, Yang D. 2007. Coxsackievirus B3 proteases 2A and 3C induce apoptotic cell death through mitochondrial injury and cleavage of eIF4GI but not DAP5/p97/NAT1. Apoptosis 12:513-24.

20. Wang Y, Zhao S, Chen Y, Wang T, Dong C, Wo X, Zhang J, Dong Y, Xu W, Feng X, Qu C, Wang Y, Zhong Z, Zhao W. 2019. The Capsid Protein VP1 of Coxsackievirus B Induces Cell Cycle Arrest by Up-Regulating Heat Shock Protein 70. Front Microbiol 10:1633.

21. Weirauch MT, Yang A, Albu M, Cote AG, Montenegro-Montero A, Drewe P, Najafabadi HS, Lambert SA, Mann I, Cook K, Zheng H, Goity A, van Bakel H, Lozano JC, Galli M, Lewsey MG, Huang E, Mukherjee T, Chen X, Reece-Hoyes JS, Govindarajan S, Shaulsky G, Walhout AJM, Bouget FY, Ratsch G, Larrondo LF, Ecker JR, Hughes TR. 2014. Determination and inference of eukaryotic transcription factor sequence specificity. Cell 158:1431-1443.

22. Wang K, Wang C, Xiao F, Wang H, Wu Z. 2008. JAK2/STAT2/STAT3 are required for myogenic differentiation. J Biol Chem 283:34029-36.

23. Lee SC, Min HY, Jung HJ, Park KH, Hyun SY, Cho J, Woo JK, Kwon SJ, Lee HJ, Johnson FM, Lee HY. 2016. Essential role of insulin-like growth factor 2 in resistance to histone deacetylase inhibitors. Oncogene 35:5515-5526.

24. Durant L, Watford WT, Ramos HL, Laurence A, Vahedi G, Wei L, Takahashi H, Sun HW, Kanno Y, Powrie F, O'Shea JJ. 2010. Diverse targets of the transcription factor STAT3 contribute to T cell pathogenicity and homeostasis. Immunity 32:605-15.

25. Carow B, Rottenberg ME. 2014. SOCS3, a Major Regulator of Infection and Inflammation. Front Immunol 5:58.

26. Akhtar LN, Benveniste EN. 2011. Viral exploitation of host SOCS protein functions.

567 J Virol 85:1912-21.

568 27. Wakahara R, Kunimoto H, Tanino K, Kojima H, Inoue A, Shintaku H, Nakajima K.
569 2012. Phospho-Ser727 of STAT3 regulates STAT3 activity by enhancing
570 dephosphorylation of phospho-Tyr705 largely through TC45. Genes Cells 17:132-45.

571 28. Lim CP, Cao X. 1999. Serine phosphorylation and negative regulation of Stat3 by
572 JNK. J Biol Chem 274:31055-61.

573 29. Gkouveris I, Nikitakis N, Karanikou M, Rassidakis G, Sklavounou A. 2014. Erk1/2
574 activation and modulation of STAT3 signaling in oral cancer. Oncol Rep 32:2175-82.

575 30. Gkouveris I, Nikitakis N, Karanikou M, Rassidakis G, Sklavounou A. 2016. JNK1/2
576 expression and modulation of STAT3 signaling in oral cancer. Oncol Lett 12:699-706.

577 31. Kecha O, Martens H, Franchimont N, Achour I, Hazee-Hagelstein MT,
578 Charlet-Renard C, Geenen V, Winkler R. 1999. Characterization of the insulin-like
579 growth factor axis in the human thymus. J Neuroendocrinol 11:435-40.

580 32. Kemball CC, Harkins S, Whitmire JK, Flynn CT, Feuer R, Whitton JL. 2009.
581 Coxsackievirus B3 inhibits antigen presentation in vivo, exerting a profound and
582 selective effect on the MHC class I pathway. PLoS Pathog 5:e1000618.

583 33. Shiu RP, Paterson JA. 1988. Characterization of insulin-like growth factor II
584 peptides secreted by explants of neonatal brain and of adult pituitary from rats.
585 Endocrinology 123:1456-60.

586 34. Qiu Q, Basak A, Mbikay M, Tsang BK, Gruslin A. 2005. Role of pro-IGF-II
587 processing by proprotein convertase 4 in human placental development. Proc Natl
588 Acad Sci U S A 102:11047-52.

589 35. St-Pierre C, Brochu S, Vanegas JR, Dumont-Lagace M, Lemieux S, Perreault C.
590 2013. Transcriptome sequencing of neonatal thymic epithelial cells. Sci Rep 3:1860.

591 36. Aguech-Oueslati L, Jaidane H, Sane F, Jrad-Battikh N, Hamed SB, Hober D,

592 Gharbi J. 2018. Evaluation of Contamination Risks with Coxsackievirus B4 E2 in Swiss
593 Albino Mice Stools. Curr Microbiol 75:32-39.

594 37. Klingel K, Stephan S, Sauter M, Zell R, McManus BM, Bultmann B, Kandolf R.
595 1996. Pathogenesis of murine enterovirus myocarditis: virus dissemination and
596 immune cell targets. J Virol 70:8888-95.

597 38. Matteucci D, Toniolo A, Conaldi PG, Basolo F, Gori Z, Bendinelli M. 1985.
598 Systemic lymphoid atrophy in coxsackievirus B3-infected mice: effects of virus and
599 immunopotentiating agents. J Infect Dis 151:1100-8.

600 39. Der SD, Zhou A, Williams BR, Silverman RH. 1998. Identification of genes
601 differentially regulated by interferon alpha, beta, or gamma using oligonucleotide
602 arrays. Proc Natl Acad Sci U S A 95:15623-8.

603 40. van Koetsveld PM, Vitale G, Feelders RA, Waaijers M, Sprij-Mooij DM, de Krijger
604 RR, Speel EJ, Hofland J, Lamberts SW, de Herder WW, Hofland LJ. 2013.
605 Interferon-beta is a potent inhibitor of cell growth and cortisol production in vitro and
606 sensitizes human adrenocortical carcinoma cells to mitotane. Endocr Relat Cancer
607 20:443-54.

608 41. Vitale G, van Koetsveld PM, de Herder WW, van der Wansem K, Janssen JA,
609 Colao A, Lombardi G, Lamberts SW, Hofland LJ. 2009. Effects of type I interferons on
610 IGF-mediated autocrine/paracrine growth of human neuroendocrine tumor cells. Am J
611 Physiol Endocrinol Metab 296:E559-66.

612 42. Yang K, Puel A, Zhang S, Eidenschenk C, Ku CL, Casrouge A, Picard C, von
613 Bernuth H, Senechal B, Plancoulaine S, Al-Hajjar S, Al-Ghonaium A, Marodi L,
614 Davidson D, Speert D, Roifman C, Garty BZ, Ozinsky A, Barrat FJ, Coffman RL, Miller
615 RL, Li X, Lebon P, Rodriguez-Gallego C, Chapel H, Geissmann F, Jouanguy E,
616 Casanova JL. 2005. Human TLR-7-, -8-, and -9-mediated induction of IFN-alpha/beta
617 and -lambda Is IRAK-4 dependent and redundant for protective immunity to viruses.
618 Immunity 23:465-78.

619 43. Erbay E, Park IH, Nuzzi PD, Schoenherr CJ, Chen J. 2003. IGF-II transcription in
620 skeletal myogenesis is controlled by mTOR and nutrients. J Cell Biol 163:931-6.

621 44. Asfari M, De W, Noel M, Holthuizen PE, Czernichow P. 1995. Insulin-like growth
622 factor-II gene expression in a rat insulin-producing beta-cell line (INS-1) is regulated
623 by glucose. Diabetologia 38:927-35.

624 45. Lee YI, Kim SJ. 1996. Transcriptional repression of human insulin-like growth
625 factor-II P4 promoter by Wilms' tumor suppressor WT1. DNA Cell Biol 15:99-104.

626 46. Wen X, Liu H, Xiao G, Liu X. 2011. Downregulation of the transcription factor KLF4
627 is required for the lineage commitment of T cells. Cell Res 21:1701-10.

628 47. An J, Golech S, Klaewsongkram J, Zhang Y, Subedi K, Huston GE, Wood WH,
629 3rd, Wersto RP, Becker KG, Swain SL, Weng N. 2011. Kruppel-like factor 4 (KLF4)
630 directly regulates proliferation in thymocyte development and IL-17 expression during
631 Th17 differentiation. FASEB J 25:3634-45.

632 48. Carlson CM, Endrizzi BT, Wu J, Ding X, Weinreich MA, Walsh ER, Wani MA,
633 Lingrel JB, Hogquist KA, Jameson SC. 2006. Kruppel-like factor 2 regulates thymocyte
634 and T-cell migration. Nature 442:299-302.

635 49. Lomada D, Jain M, Bolner M, Reeh KA, Kang R, Reddy MC, DiGiovanni J, Richie
636 ER. 2016. Stat3 Signaling Promotes Survival And Maintenance Of Medullary Thymic
637 Epithelial Cells. PLoS Genet 12:e1005777.

638 50. Satoh R, Kakugawa K, Yasuda T, Yoshida H, Sibilia M, Katsura Y, Levi B,
639 Abramson J, Koseki Y, Koseki H, van Ewijk W, Hollander GA, Kawamoto H. 2016.
640 Requirement of Stat3 Signaling in the Postnatal Development of Thymic Medullary
641 Epithelial Cells. PLoS Genet 12:e1005776.

642 51. Chang Z, Wang Y, Bian L, Liu Q, Long JE. 2017. Enterovirus 71 antagonizes the
643 antiviral activity of host STAT3 and IL-6R with partial dependence on virus-induced
644 miR-124. J Gen Virol 98:3008-3025.

645 52. Kiuchi N, Nakajima K, Ichiba M, Fukada T, Narimatsu M, Mizuno K, Hibi M, Hirano
646 T. 1999. STAT3 is required for the gp130-mediated full activation of the c-myc gene. J
647 Exp Med 189:63-73.

648 53. Luo H, Yanagawa B, Zhang J, Luo Z, Zhang M, Esfandiarei M, Carthy C, Wilson
649 JE, Yang D, McManus BM. 2002. Coxsackievirus B3 replication is reduced by
650 inhibition of the extracellular signal-regulated kinase (ERK) signaling pathway. J
651 Virol 76:3365-73.

652 54. Si X, Luo H, Morgan A, Zhang J, Wong J, Yuan J, Esfandiarei M, Gao G, Cheung
653 C, McManus BM. 2005. Stress-activated protein kinases are involved in coxsackievirus
654 B3 viral progeny release. J Virol 79:13875-81.

655 55. Zhu M, Duan H, Gao M, Zhang H, Peng Y. 2015. Both ERK1 and ERK2 are
656 required for enterovirus 71 (EV71) efficient replication. Viruses 7:1344-56.

657 56. Andersson P, Alm S, Edman K, Lindberg AM. 2005. A novel and rapid method to
658 quantify cytolytic replication of picornaviruses in cell culture. J Virol Methods
659 130:117-23.

660 57. Pourianfar HR, Javadi A, Grollo L. 2012. A colorimetric-based accurate method for
661 the determination of enterovirus 71 titer. Indian J Virol 23:303-10.

662 58. Rotwein P, Hall LJ. 1990. Evolution of insulin-like growth factor II: characterization
663 of the mouse IGF-II gene and identification of two pseudo-exons. DNA Cell Biol
664 9:725-35.

665 59. Caricasole A, Ward A. 1993. Transactivation of mouse insulin-like growth factor II
666 (IGF-II) gene promoters by the AP-1 complex. Nucleic Acids Res 21:1873-9.

667 60. Dreos R, Ambrosini G, Cavin Perier R, Bucher P. 2013. EPD and EPDnew,
668 high-quality promoter resources in the next-generation sequencing era. Nucleic Acids
669 Res 41:D157-64.

670

671 **FIGURE LEGENDS**
672

673 **Fig. 1 Effect of CV-B4 E2 on murine thymic *Igf2* mRNA isoforms and its precursors**
674 ***in vivo.*** (**A**) Schematic thymus processing for isolation of total thymic cells (unsorted
675 cells) and $CD45^-$ enriched cells (TECs). (**B**) Flow cytometry analysis of CD45 enriched
676 TECs ($EpCAM^+CD45^-$) *versus* unsorted total thymic population. Numbers indicate the
677 percentage of TECs population (**C**) Relative mRNA expression of *total Igf2* mRNA in
678 unsorted total thymic population and in matched enriched TECs fraction (CD45-). Mock
679 uninfected mice at day 2 P.I. were used; *n* = 6. (**D**) Relative mRNA expression of *Igf2 V3,*
680 *V1 and V2* mRNA transcripts isoforms in $CD45^-$ enriched TECs in mock uninfected mice
681 at day 3 P.I. For each sample, relative mRNA expression of *Igf2* transcripts isoforms was
682 normalized to the corresponding *total Igf2* mRNA expression; *n* = 6 (**E**) Relative mRNA
683 expression of *Igf2* mRNA isoforms in mock and in CV-B4 E2 infected mice;
684 box-and-whisker plots extend from minimum to maximum values, with lines at medians;
685 *n* = 5-6 (**F**) Left panel, representative Western blot of IGF2 and its precursors at day 7 P.I.
686 in mock (-) and in CV-B4 E2 infected mice (+). Independent biological samples are
687 represented. PC, purified mature IGF2. Right panel, relative quantification of pro-IGF2 in
688 mock and in CV-B4 E2 infected mice; histogram represents mean of relative value ± SD;
689 *n* = 3. (**G**) Representative agarose gel electrophoresis of one-step RT-PCR products of
690 CV-B4 E2 genome in digested thymus (total thymic cells) and in matched pancreas, in
691 CV-B4 E2 (+) or in mock uninfected mice (-). Independent biological samples are shown.
692 L, ladder; PC, MTE4-14 cells infected with CV-B4 E2. (**C**) Student's paired *t* test,
693 $^{**}p < 0.01$ (**E-F**) Student's *t* test, $^{**}p < 0.01$ and $^{*}p < 0.05$; (**D; F**) one-way ANOVA,
694 $^{**}p < 0.01$; $\#p < 0.05$.

Fig. 2 *Igf2* mRNA isoforms expression in MTE4-14 cell line. (**A**) RT-PCR of *Igf2 V1* (90 bp), *Igf2 V2* (98 bp), *Igf2 V3* (68 bp), *total Igf2* (107 bp). Mock sample from 2 independent experiments are represented, murine brain is used as positive control. (**B**) Relative mRNA expression of *Igf2 V1* and *Igf2 V3* (n = 6); relative expression was normalized to *Hprt* with $E^{-\Delta Ct}$ formula (with E represents efficiency amplification for *Igf2 V3* and *Igf2 V1);* box-and-whisker plots extend from minimum to maximum values with lines at medians. Student t test, $*p < 0.05$.

Fig. 3 Effect of CV-B4 E2 on *Igf2* at mRNA and its precursors on MTE4-14. (**A**) Fold change of mRNA expression of *Igf2* transcripts in CV-B4 E2 $_{MOI = 0.05}$ infected cells relative to matched mock uninfected cells (n = 6-12); mock samples are represented as a dashed line set at y = 1; box-and-whisker plots (CV-B4 E2 $_{MOI = 0.05}$ infected cells) extend from minimum to maximum values, with lines at medians.(**B**) Fold change mRNA expression of *Tp53, Birc5 and Bax* in CV-B4 E2 $_{MOI = 0.05}$ infected cells relative to matched mock uninfected cells at day 3 P.I. Mock samples are represented as a dashed line set at y = 1; data are represented as mean of fold change ± SEM; n = 3 (**C**) Left panel, Western blot analysis of IGF2 and its precursors in CV-B4 E2 infected cells (+) and in mock uninfected cells (-). PC, purified mature IGF2. Right panel, relative quantification of pro-IGF2 in CV-B4 E2 $_{MOI = 0.05}$ infected cells (grey histograms) normalized to matched mock uninfected cells (white histograms) (n = 3); histogram represents mean of fold change ± SEM. (**D**) Representative agarose gel electrophoresis of amplicons specific to the positive and negative strands of CV-B4 E2 genome (155 bp), amplified by semi-nested strand specific RT-PCR, from CV-B4 E2 $_{MOI = 0.05}$ infected MTE4-14 cells; mock samples served as negative control. (**E**) Representative Western blot analysis of VP1 in CV-B4 E2 $_{MOI = 0.05}$

infected MTE4-14 cells (+) or mock uninfected cells (-). Data are representative of three independent experiments. (**F**) Viral titer of CV-B4 E2 $_{MOI = 0.05}$ in MTE4-14 infected cells. Mean of $TCID_{50}$/mL ± SEM (*n* = *3*-5) are shown. (**A-C**) ratio paired *t* test, ***$p < 0.001$ and *$p < 0.05$; (**A, C**) one-way ANOVA, #$p < 0.05$; (**F**) Kruskal-Wallis test, ###$p<0.001$.

Fig. 4 Effect of CV-B4 E2 on *Igf2* P3 promoter activity in MTE4-14 and on *Igf2* transcript stability. (**A**) Sequence of the murine *Igf2 P3* promoter sequence (-168/+175) https://epd.epfl.ch. The restriction site *NheI* and *EcoRV* are indicated above in italic. The transcription start site is represented by an arrow at +1. (**B**) Nanoluciferase relative activity of *Igf2 P3* promoter (-168/+175) after 1 (left panel) and 2 days P.I. (right panel). Analysis was realized as described in methods. Mean of relative dual-luciferase activity normalized to mock are represented ± SEM. (**C**) mRNA half-life of *Igf2 V3* transcripts in CV-B4 E2 $_{MOI = 0.05}$ or mock uninfected cells at day 2 P.I. followed by 2-10 hours of treatment with actinomycin D (*n* = 4), vehicle control was used for data normalization for each time point. (**B-C**) ratio paired *t* test, ***$p < 0.001$ and *$p < 0.05$; (**B**) one-way ANOVA, #$p < 0.05$.

Fig. 5 Deletion analysis of *Igf2* P3 promoter in MTE4-14 cells infected with CV-B4 E2 $_{MOI = 0.05}$. (**A**) Schematic representation of the *Igf2* P3 promoter constructs in Nanoluciferase vector. (**B-C**) Nanoluciferase relative activity of *Igf2 P3* promoter constructs at day 2 P.I. in CV-B4 E2 $_{MOI = 0.05}$ or in mock uninfected cells, transfected by the indicated *Igf2* P3 promoter construct. Mean of relative dual-luciferase activity normalized to mock are represented ± SEM. Mock uninfected cells transfected by the full *Igf2* P3 promoter (-168/+175) is set at 100% in each experiment (*n* = 4-16).

Ratio paired *t* test, *$p < 0.05$, ***$p < 0.001$.

Fig. 6 Effect of CV-B4 E2 on STAT3 phosphorylation and on STAT3 signaling pathway. (**A**) Left panel, Western blot analysis of $STAT3^{total}$ and $STAT3^{pY705}$ in CV-B4 E2 infected cells (+) and in matched mock uninfected cells (-). Right panel, relative quantification of $STAT3^{total}$ and $STAT3^{pY705}$ in CV-B4 E2 $_{MOI = 0.05}$ infected cells (+) and in day matched mock uninfected cells (-) (*n* = 4-5); box-and-whisker plots representing CV-B4 E2 $_{MOI = 0.05}$ infected cells, extend from minimum to maximum values, with lines at medians; mock samples are represented as a dashed line set at y = 1. (**B**) Fold change of *Bcl2* mRNA in CV-B4 E2 $_{MOI = 0.05}$ infected cells (grey histograms) relative to matched mock uninfected cells (white histograms); n = 3-6. (**C**) *Il6* mRNA relative expression in CV-B4 E2 $_{MOI = 0.05}$ infected cells (+) and in matched mock uninfected cells (-); *n* = 6. (**D**) Quantification of extracellular IL-6Rα by flow cytometry in CV-B4 E2 $_{MOI = 0.05}$ infected cells (+) and in matched mock uninfected cells (-); data are represented as MFI value relative to isotype control; *n* = *4*-5. (**E**) Left panel, Western blot analysis of SOCS3 in CV-B4 E2 $_{MOI = 0.05}$ infected cells (+) in day matched mock uninfected cells (-). Right panel, relative quantification of SOCS3 in CV-B4 E2 $_{MOI = 0.05}$ infected cells (+) and in day matched mock uninfected cells (-); *n* = *2*-3. (**F**) Left panel, Western blot analysis of JNK^{total} and phosphorylated JNK in CV-B4 E2 $_{MOI = 0.05}$ infected cells (+) and in matched mock uninfected cells (-); two independent experiments are represented. Right panel, relative quantification of JNK^{total} and phosphorylated JNK in CV-B4 E2 $_{MOI = 0.05}$ infected cells (+) and in matched mock uninfected cells (-); *n* = 3. (**G**) Left panel, Western blot analysis of total ERK and p-ERK in CV-B4 E2 $_{MOI = 0.05}$ infected cells (+) and in matched mock uninfected cells (-). Right panel, relative quantification of ERK^{total} and phosphorylated ERK in CV-B4 E2 $_{MOI = 0.05}$ infected cells (+) and in matched mock uninfected cells (-); *n* = 1. (**B**, **E, F-G**) Histograms represents average ± SEM. (**A-F**), Ratio paired *t* test,

765 **$p < 0.01$ and *$p < 0.05$; (**A-B**) one-way ANOVA, #$p < 0.05$.

766

767 **Table 1. Putative transcription factor binding site in the region -68/-22 and**
768 **-168/-116.**

Murine *Igf2 P3* (-68 to -22)			
Name	**Motif ID**	**GeneID**	**Score**
Klf6	M08857_2.00	ENSMUSG00000000078	16.87
Klf4	M08857_2.00	ENSMUSG00000003032	16.87
Klf5	M08857_2.00	ENSMUSG00000005148	16.87
Klf7	M08857_2.00	ENSMUSG00000025959	16.87
Klf3	M08857_2.00	ENSMUSG00000029178	16.87
Klf1	M08857_2.00	ENSMUSG00000054191	16.87
Klf2	M08857_2.00	ENSMUSG00000055148	16.87
Klf12	M08857_2.00	ENSMUSG00000072294	16.87
Klf15	M08907_2.00	ENSMUSG00000030087	16.49
Patz1	M08864_2.00	ENSMUSG00000020453	15.798
Klf8	M08871_2.00	ENSMUSG00000041649	14.828
Sp1	M09016_2.00	ENSMUSG00000001280	16.03
Sp4	M09016_2.00	ENSMUSG00000025323	16.03
Sp3	M09016_2.00	ENSMUSG00000027109	16.03
Sp6	M09016_2.00	ENSMUSG00000038560	16.03
Sp8	M09016_2.00	ENSMUSG00000048562	16.03
Sp9	M09016_2.00	ENSMUSG00000068859	16.03
Sp5	M09016_2.00	ENSMUSG00000075304	16.03
Zfp341	M08892_2.00	ENSMUSG00000059842	15.256
Zfp263	M08272_2.00	ENSMUSG00000022529	14.357
Q8K439_MOUSE	M08272_2.00	Q8K439_MOUSE	14.357
Nkx2-1	M08136_2.00	ENSMUSG00000001496	13.307
Nkx2-5	M08136_2.00	ENSMUSG00000015579	13.307
Nkx2-2	M08136_2.00	ENSMUSG00000027434	13.307
Nkx2-6	M08136_2.00	ENSMUSG00000044186	13.307
Nkx2-3	M08136_2.00	ENSMUSG00000044220	13.307
Nkx2-4	M08136_2.00	ENSMUSG00000054160	13.307
Nkx2-9	M08136_2.00	ENSMUSG00000058669	13.307

769

770

771

772

773

774

Murine *Igf2 P3* (-168 to -116)

Name	Motif ID	GeneID	Score
Zfp263	M08082_2.00	ENSMUSG00000022529	14.251
Q8K439_MOUSE	M08082_2.00	Q8K439_MOUSE	14.251
Maz	M08988_2.00	ENSMUSG00000030678	13.087
Prdm5	M08986_2.00	ENSMUSG00000029913	13.783
Zfp383	M07689_2.00	ENSMUSG00000099689	13.452
Sp1	M09016_2.00	ENSMUSG00000001280	15.157
Sp4	M09016_2.00	ENSMUSG00000025323	15.157
Sp3	M09016_2.00	ENSMUSG00000027109	15.157
Sp6	M09016_2.00	ENSMUSG00000038560	15.157
Sp8	M09016_2.00	ENSMUSG00000048562	15.157
Sp9	M09016_2.00	ENSMUSG00000068859	15.157
Sp5	M09016_2.00	ENSMUSG00000075304	15.157
Etv3	M09055_2.00	ENSMUSG00000003382	13.617
Etv1	M09055_2.00	ENSMUSG00000004151	13.617
Etv2	M09055_2.00	ENSMUSG00000006311	13.617
Elk3	M09055_2.00	ENSMUSG00000008398	13.617
Gabpa	M09055_2.00	ENSMUSG00000008976	13.617
Elk1	M09055_2.00	ENSMUSG00000009406	13.617
Etv5	M09055_2.00	ENSMUSG00000013089	13.617
Fli1	M09055_2.00	ENSMUSG00000016087	13.617
Etv4	M09055_2.00	ENSMUSG00000017724	13.617
Ets2	M09055_2.00	ENSMUSG00000022895	13.617
Elk4	M09055_2.00	ENSMUSG00000026436	13.617
Elf4	M09055_2.00	ENSMUSG00000031103	13.617
Ets1	M09055_2.00	ENSMUSG00000032035	13.617
Elf1	M09055_2.00	ENSMUSG00000036461	13.617
Elf2	M09055_2.00	ENSMUSG00000037174	13.617
Erg	M09055_2.00	ENSMUSG00000040732	13.617
Erf	M09055_2.00	ENSMUSG00000040857	13.617
Fev	M09055_2.00	ENSMUSG00000055197	13.617
XP_911724.4	M09055_2.00	XP_911724.4	13.617
Zfp263	M07844_2.00	ENSMUSG00000022529	16.224
Q8K439_MOUSE	M07844_2.00	Q8K439_MOUSE	16.224
Zfp281	M08999_2.00	ENSMUSG00000041483	13.023
E2f4	M09034_2.00	ENSMUSG00000014859	14.084
E2f3	M09034_2.00	ENSMUSG00000016477	14.084
E2f2	M09034_2.00	ENSMUSG00000018983	14.084
E2f1	M09034_2.00	ENSMUSG00000027490	14.084
E2f5	M09034_2.00	ENSMUSG00000027552	14.084
E2f6	M09034_2.00	ENSMUSG00000057469	14.084
Sall4	M08866_2.00	ENSMUSG00000027547	13.786
Patz1	M08287_2.00	ENSMUSG00000020453	14.129

775

776 **Table 2. CV-B4 E2 mRNA detection by RT-PCR performed in other studies.**

Tissue	Days P.I.					Study	Processing	Viral dose ($TCID_{50}$)	Inoculation method
	2	3	7	8	10				
Pancreas	2/2	2/2	2/2	n/a	2/2	*Jaïdane et. al,* [2006]	WT	$10^{4.74}$	Oral
	n/a	n/a	n/a	2/2	n/a	*Aguech-Oueslati et. al*, [2017]	WT	10^{5}	Oral I.P.
	6/6	6/6	2/6	n/a	n/a	Actual study	WT	10^{6}	I.P.
Thymus	2/2	2/2	2/2	n/a	1/2	*Jaïdane et. al,* [2006]	WT	$10^{4.74}$	Oral
	n/a	n/a	n/a	2/2	n/a	*Aguech-Oueslati et. al,* [2017]	WT	10^{5}	Oral + I.P.
	0/6	0/6	0/6	n/a	n/a	Actual study	EP	10^{6}	I.P.

WT, whole tissue; EP, enzymatic processing; I.P., intra-peritoneal; n/a, no data; 2/2 represents two positive samples for two independent biological samples tested

777

778

779

780

781

782

783

784

785

786

787

Table 3. Sequences of qPCR primers, site-directed mutagenesis primers

Table 3-1. qPCR primers sequence

Gene	Sequence 5'-3'	PCR product size (bp)
Hprt	Forward: TTATCAGACTGAAGAGCTACTGTAATG Reverse: CTTCAACAATCAAGACATTCTTTCC	108
Igf2 (total)	Forward: GGGAGCTTGTGGACACGC Reverse: GCACTCTTCCACGATGCCA	107
Igf2 V1	Forward: CCGGCTTCCAGGTACCAAT Reverse: GCAGCGATGCAGCACAAG	91
Igf2 V2	Forward: GCCCTTCTCCTCCGATCCT Reverse: ATGAGAAGCACCAACATCGACTT	99
Igf2 V3	Forward: CCAGCCTTTTCCTGTCTTCATC reverse: CCATTGGTACCTGAAGTTGGGTAA	69
Birc5	Forward: TCTGGCAGCTGTACCTCAAGAACT Reverse: AAACACTGGGCCAAATCAGGCT	148
Tp53	Forward: TTCATTGGGACCATCCTGGC Reverse: TGGCAGTCATCCAGTCTTCG	121
Bcl2	Forward: GTGAACTGGGGGAGGATTGT Reverse: GGAGAAATCAAACAGAGGCC	216
Il6	Forward: GTTCTCTGGGAAATCGTGGA Reverse: TGTACTCCAGGTAGCTATGG	208

795 **Table 3-2. Site-directed mutagenesis primers sequence**

Igf2 P3 **plasmid (sequence relative to TSS)**	**Primer**	**Annealing (°C)**
P243 -68/+175	Forward: GGTAGGGTGGAGCCGGGA Reverse: GAGCTCAGGTACCGGCCA	68°C
P149 +26/+175	Forward: AACCTTCCAGCCTTTTCCTGT Reverse: GAGCTCAGGTACCGGCCA	66°C
P98 +77/+175	Forward TTACCCAACTTCAGGTAACCAGG Reverse: GAGCTCAGGTACCGGCCA	70°C
P197 -22/+175	Forward: GGAGGCACTGACCAGTTCG Reverse: GAGCTCAGGTACCGGCCA	67°C
P169 +6/+175	Forward: ACATTAGCTTCTCCTGTGAGAAC Reverse: GAGCTCAGGTACCGGCCA	65°C
P291 -116/+175	Forward : GCGGGTGCAAAGGGGGCG Reverse: GAGCTCAGGTACCGGCCAGTTAG	70°C
P230 -55/+175	Forward : GGGACTGGGAGGAGCCAC Reverse: GAGCTCAGGTACCGGCCA	71°C
P248* -167/-116$^{\Delta-116/-22}$-22/+175	Forward : CGGAGGCACTGACCAGTTC Reverse: CCCCTCCCTCCTTCCAGC	67°C
P307* -167/-151$^{\Delta-151/-116}$-116/+175	Forward: GGCGGGTGCAAAGGGGGC Reverse: CACCCCCAAGAGCTAGCGAGC	69°C
Sequencing primer	Forward: CTAGCAAAATAGGCTGTCCC Reverse:ACTGCATTCTAGTTGTGGTTTGC	

796

797

798

799

800 **Table 4. List of antibody used for Western Blot**

Primary antibody	Dilution	Supplier	Clone
Rabbit anti-IGF2	1:500	AVIVA SYSTEMS BIOLOGY	OAAB07463
Rabbit anti-STAT3	1:1000	Cell Signaling Technology	D3Z2G
Rabbit anti-STAT3 (p705 Tyr)	1:1000	Cell Signaling Technology	D3A7
Rabbit anti-JNK/SAPK	1:1000	Cell Signaling Technology	
Rabbit anti-pJNK	1:1000	Cell Signaling Technology	81E11
Rabbit anti-ERK (1/2)	1:1000	Cell Signaling Technology	137F5
Rabbit anti-pERK (1/2)	1:1000	Cell Signaling Technology	Anti-rabbit IgG HRP
Rabbit anti-SOCS3	1:1000	Cell Signaling Technology	Anti-rabbit IgG HRP
Mouse anti-GAPDH	1:1000	Pierce	GA1R
Mouse anti-β tubulin	1:1000	Pierce	BT7R
Mouse anti-VP1	1:1000	Dako	5-D8/1

801

802

803

804

805

806

807

808

809

810

811

812

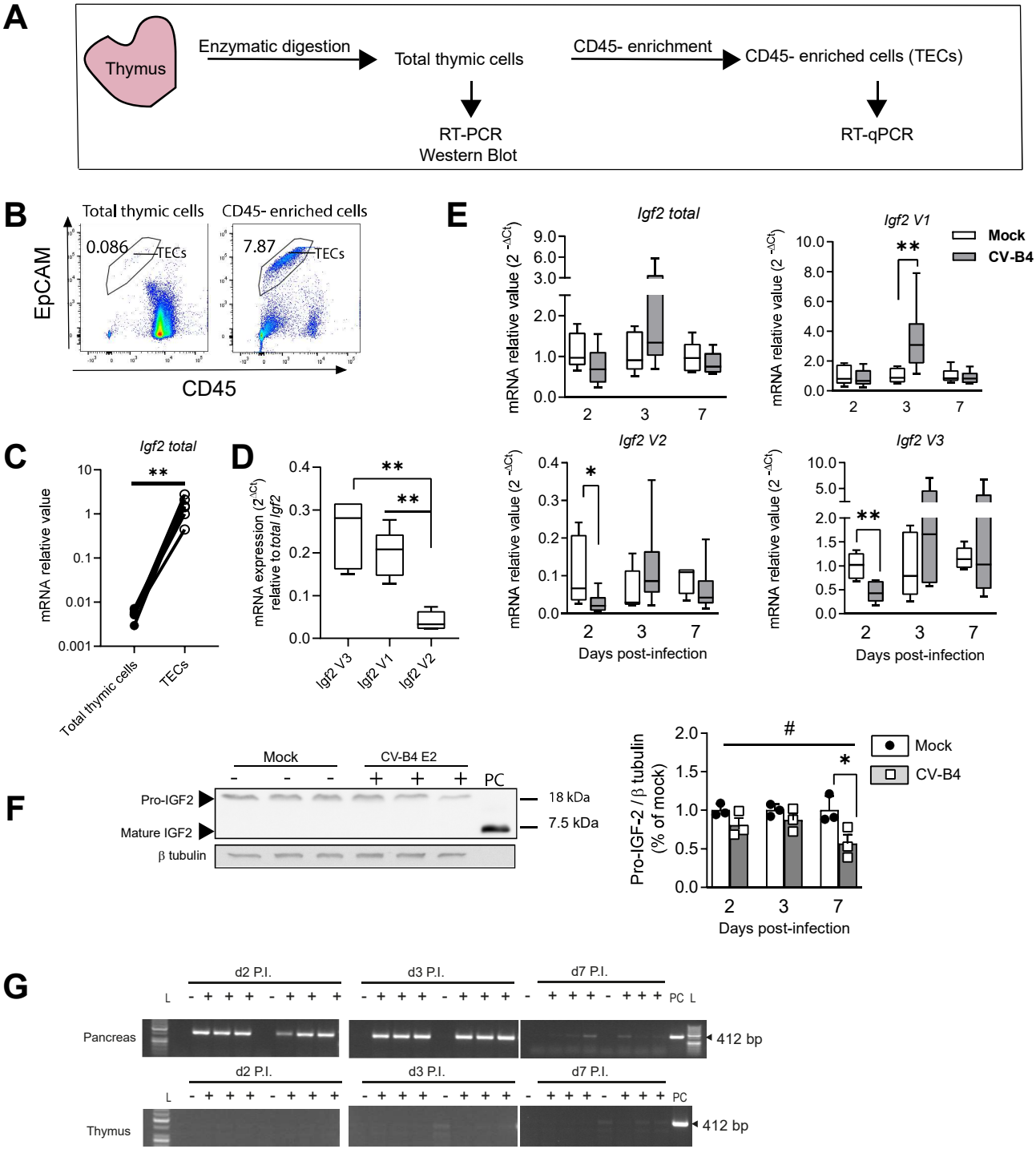

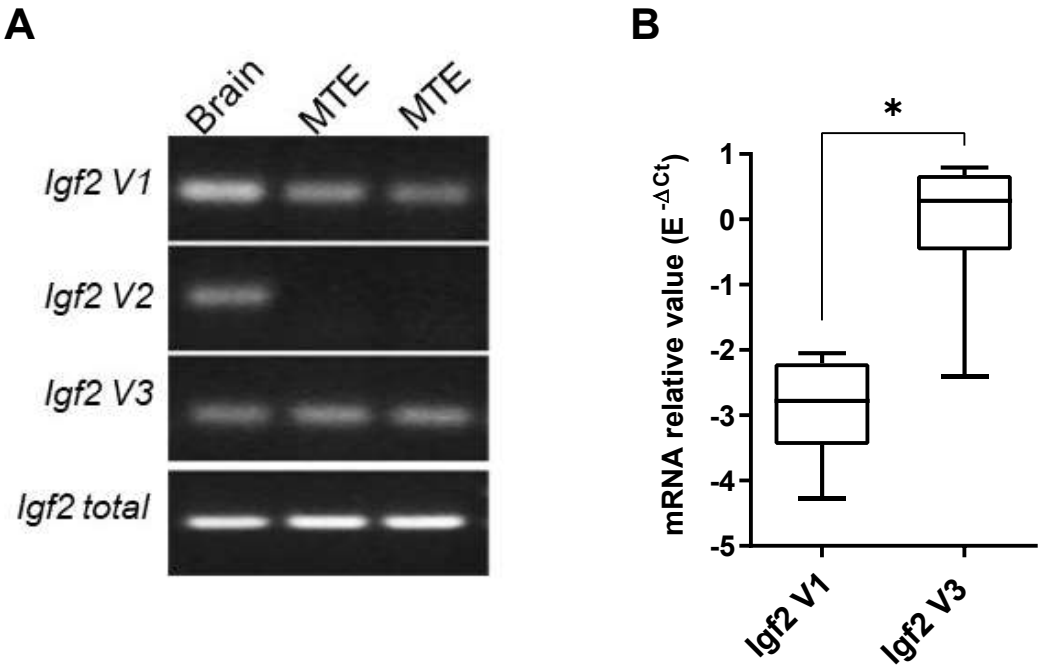

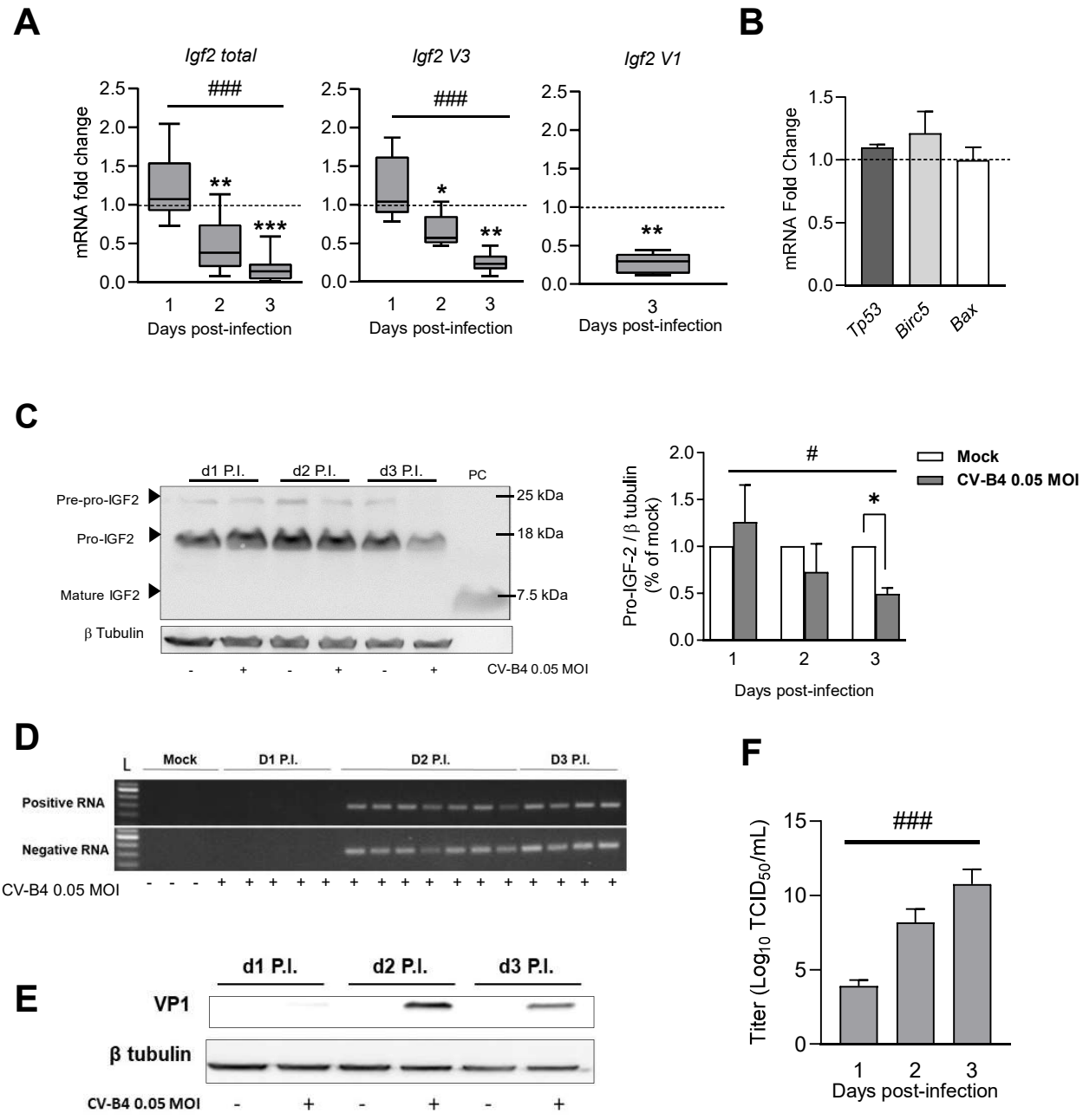

A

```
    NheI
1   GCTAGCTCTT GGGGGTGCAG GAGAAAAGGG ACTGGCTGGA AGGAGGGAGG
-168
50  GGGCGGGTGC AAAGGGGGCG GGGGGAGTGG TCAGCAGGGA GGGGGTGGGG

100 GGTAGGGTGG AGCCGGGACT GGGAGGAGCC ACTCAGACAT AAAAAGCGGA

150 GGCACTGACC AGTTCGCAAA CTGGACATTA GCTTCTCCTG TGAGAACCTT
                    +1
200 CCAGCCTTTT CCTGTCTTCA TCCTCTTCCA GCCCCAGCGG CCTCCTTACC

250 CAACTTCAGG TAACCAGGGC TGTGGAGCCA GGACCCTGCT GCCATCCCCA
                                                  EcoRV
300 CTCCGGCTTG CCCAGTGGGG TGGTCAGGGC ACCGGGTAGC CTGGATATC
                                                 +175
```

B

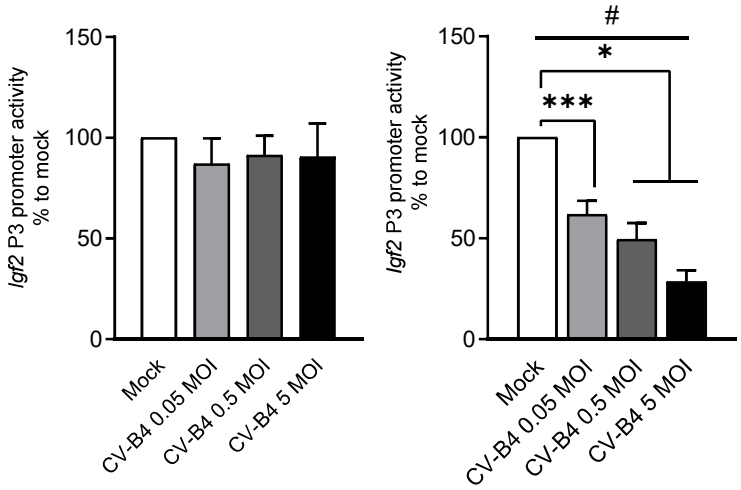

C